Journal of Membrane Science 713 (2025) 123380

Contents lists available at ScienceDirect

Journal of Membrane Science

journal homepage: www.elsevier.com/locate/memsci

Single particle tracking reveals through-membrane diffusion of bacteriophage during process disruption of virus filtration

Ian Wyllie [a], Mohammad A. Afzal [b], Anni Shi [a], Andrew L. Zydney [b], Daniel K. Schwartz [a,*]

[a] Department of Chemical and Biological Engineering, University of Colorado Boulder, Boulder, CO, 80309, USA
[b] Department of Chemical Engineering, The Pennsylvania State University, University Park, PA, 16802, USA

ARTICLE INFO

Keywords:
Virus filtration
Single particle tracking
Mass transport
Diffusion

ABSTRACT

In the biopharmaceutical industry, virus filters are crucial for ensuring the removal of endogenous and adventitious viruses as part of the viral clearance strategy. Although traditionally described as a size-exclusion mechanism, virus retention has a process-dependent nature where challenging conditions, such as process disruptions, may compromise membrane retention and significantly increase virus filtrate concentrations. The detailed mechanisms underlying this loss of retention are challenging to determine using traditional breakthrough experiments. In this work, single particle tracking and kinetic simulations were employed to connect individual particle behavior to the observed macroscopic losses in virus retention. Our experiments, using fluorescently labeled ΦX174 bacteriophage as a model parvovirus, replicated conditions representative of process disruptions within the Pegasus SV4, a homogeneous polymeric virus filtration membrane. During flow, phage particles retained were trapped within relatively large cavity spaces that had downstream constrictions aligned with the flow direction; the trapped particles were dynamic and exhibited significant intra-cavity motion. Upon flow stoppage, particles escaped from these retention locations rapidly, with approximately 90 % of previously trapped particles being remobilized for process disruption times ranging from 2 to 10 min, suggesting that local cavity escape had reached saturation at these timescales. Diffusion experiments within the membrane revealed isotropic and Fickian motion, hindered by more than an order of magnitude compared to diffusion in unconfined liquid. Despite the reduced mobility within the membrane, the substantial diffusion coefficient of 4.19 ± 0.06 $\mu m^2/s$ indicated that virus particles could travel tortuous but non-retentive pathways through the membrane on length scales equal to or greater than the membrane thickness during a disruption event. A 1D kinetic Monte-Carlo simulation successfully connected single-particle behavior to macroscopically observed virus release, indicating that significant diffusive release into the filtrate can occur even without the resumption of flow. This work provides crucial insights into the retention behavior of homogeneous membranes during periods of disruption, enabling the design of more robust mitigation strategies and filter designs.

1. Introduction

The production of recombinant protein therapeutics, including monoclonal antibodies derived from CHO cells, is a rapidly expanding sector within the biopharmaceutical industry. In 2020, the monoclonal antibody market alone was valued at $154 billion and is projected to double by 2025 [1,2]. To ensure public health and safety, regulatory agencies impose strict criteria for the removal of viral contaminants within the downstream purification [1,3,4]. At least two orthogonal modes of viral clearance are necessary to remove both larger retrovirus-like particles (~50–120 nm in diameter) and smaller parvoviruses (~20 nm) of endogenous and adventitious origins [1,5].

Within industry, virus filtration (VF) devices are commonly used in combination with inactivation and adsorptive removal steps [4,5]. Typically made from porous polymeric materials, virus filters feature a network of larger cavities and constricting holes [6–8]. The intricate pore structure creates a tortuous environment that, simplistically, removes particles based on size exclusion under flow conditions. VF devices are typically employed in a multi-layer flat sheet configuration or as a hollow fiber [1,4]. These devices may exhibit either homogeneous or asymmetrically graded pore size distributions along the flow direction. Despite the variety in configurations and materials, all devices

* Corresponding author. Department of Chemical and Biological Engineering, University of Colorado, Boulder, CO, 80303, USA.
E-mail address: daniel.schwartz@colorado.edu (D.K. Schwartz).

https://doi.org/10.1016/j.memsci.2024.123380
Received 4 August 2024; Received in revised form 17 September 2024; Accepted 30 September 2024
Available online 1 October 2024

are highly effective during normal consistent flow conditions. They are engineered to provide more than a 4-log reduction value (LRV) in virus clearance (99.99 % virus retention) while maintaining over 95 % product recovery [1,4,8,9]. This efficiency is achieved even for biotherapeutics that are smaller by less than a factor of two than the smallest virus [1,5].

However, previous studies have indicated that the retentive properties of VF devices are process-dependent, suggesting a more nuanced mechanism for retention [3,4,7,9–12]. Current research in the VF community is focused on understanding the factors that lead to loss of virus retention under challenging conditions such as high virus loading [5,13,14], membrane fouling [9,15–17], and reduced filtrate flux [3,4,7,10–12,18]. Process disruptions in VF devices often occur during routine operations like switching feed tanks, shift changes, and buffer flushes to recover residual product [4,10,12,19]. Although these interruptions are difficult to avoid, they can lead to significant virus breakthrough, contaminating downstream products and resulting in economic losses [9,11]. Currently, a variety of ensemble-level experimental methods (e.g., breakthrough curve and confocal imaging) and mathematical modeling have been employed to understand these losses in retention during process disruptions.

Yamamoto et al. [7] have proposed that virus particles are retained through hydrodynamic constraint within cavities of the pore network that feature constricting holes aligned in the flow direction, preventing movement by size exclusion. Under normal process conditions, the pore-network can create substantial retention in VF devices. For homogenous style membranes, a large amount of retention is observed to occur at or near the inlet side, in what is known as the reservoir zone [4,5,12]. However, upon flow stoppage, significant virus release has been observed, characterized by up to a 1000-fold decrease in retention and deeper migration of the captured virus into the depth of the membrane for process disruptions of 2–30 min [3,4,11,12]. Additionally, these studies have extended the internal polarization model describing VF retention to include the effects of filtrate flux, including process disruption [3,12]. It has been proposed that weakly constrained virus particles can diffuse laterally, increasing the chance of reaching cavities containing non-retentive holes thereby facilitating breakthrough [3,4,7,10–12]. This diffusive escape mechanism, as outlined in the literature, specifically proposes that flow resumption after diffusion is the mechanism for the release of virus particles into the filtrate. Although considerable progress has been made in understanding the behavior of virus particles during process disruptions, the full extent of virus diffusion within VF devices and the behavior of virus particles under these conditions is not entirely understood.

Single Particle Tracking (SPT) offers researchers the ability to observe individual spatiotemporal trajectories with high resolution, enabling direct observation of complex particle dynamics [19–21]. Due to its capacity to analyze large trajectory datasets, SPT can relate rare single particle events to broader macroscopic phenomena, complementing traditional ensemble-level measurements and mathematical modeling [20]. Additionally, employing refractive index (RI) matching liquids facilitates the study of particle transport deep within porous media, overcoming light scattering effects. Furthermore, SPT has been employed to provide mechanistic insights into process dependent phenomena such as particle remobilization, membrane tortuosity, and fouling [18,19,21,22]. Notably, Wu et al. [19], studied flow stoppage-induced remobilization of 40 nm tracers in a 650 nm nominal pore size membrane. Remobilization was found to occur by diffusion, where transport on length-scales similar to the physical cavity size of the membrane resulted in particle escape following the resumption of flow. Although their study featured a system with significant variance between particle and pore sizes (where retention was a relatively rare event), it provided the groundwork for the methodologies employed in this study, which examines remobilization in a system where the nominal pore size and particle size are closely matched.

In this study, we investigated the relationship between the duration of process disruptions and virus breakthrough using Single Particle Tracking (SPT) and computational simulations. Experiments were conducted using a single layer of the Pegasus SV4 membrane, and the transport of Atto-647 N labeled ΦX174 was analyzed under both flow and quiescent conditions. SPT experiments indicated that remobilization from individual retention sites occurred significantly faster than timescales associated with macroscopic, ensemble-level breakthrough, suggesting that local escape from cavities is not the rate limiting factor. While the virus diffusion coefficient was reduced by a factor of ~30 compared to its rate in bulk, virus particles diffused both laterally and through the membrane at similar rates and were observed to travel distances comparable to the membrane's thickness during periods of process disruption; this characteristic length of transport suggested that particles escaped diffusively and did not require flow resumption for the release of viruses into the filtrate. Kinetic Monte Carlo simulations of in-membrane diffusion validated the impact of individual particle diffusion on the ensemble-level release fraction during periods of process disruption. These findings provide new insights into the process-dependent behavior of commercially available virus filters that can inform the development of more effective virus filtration strategies and membrane designs.

2. Experimental methods

2.1. Single particle tracking experiments

A polydimethylsiloxane (PDMS) flow cell device was prepared following the method described by Wu et al. [19], with minor modifications (Fig. S1). Initially, a 10:1 wt ratio of PDMS elastomer base to curing agent was mixed and poured over a master mold to form a channel. This assembly was then thermally cured at 60 °C for 3 h. To prepare the microfluidic device for imaging, a single layer of polyvinylidene fluoride (PVDF) Pegasus SV4 membrane (Pall Life Sciences, now Cytiva) was inserted orthogonally to the flow direction after making an incision, and inlet and outlet holes were punched at both ends. Pegasus SV4 is a homogenous membrane with a nominal pore size of 20 nm; SEM images of the membrane structure can be found in Fig. S2. The PDMS mold was then bonded to a glass slide using an optical adhesive (Norland Optical Adhesive), applied by spin coating at 2000 rpm for 30 s, followed by UV-ozone treatment for 5 min and thermal curing at 80 °C for 30 min.

For the process disruption experiments, fluorescently labeled phage suspended within an RI-matching solution was used. The ΦX174 bacteriophage (ATCC) was covalently conjugated with the Atto-647 N (MilliporeSignma) fluorophore using a labeling kit provided by the dye manufacturer. 1 mL of highly concentrated phage solution, with a concentration of 2.5×10^{10} plaque-forming units per mL (pfu/mL), in bicarbonate buffer was added to a vial of Atto-647 N dye mixed with 20 μL DMSO. The reaction mixture was incubated for 2 h in the dark with gentle stirring, then purified via diafiltration using a 10 kDa centrifugal concentrator (MilliporeSigma) to remove any free unreacted dye. The purified phage (1×10^{10} pfu/mL) was suspended in a solution of glycerol and PBS in a 62 %/38 % volume ratio that was passed through a 0.22 μm filter to remove larger aggregates. This bacteriophage was selected for its size and surface charge similarities to the minute-virus of mice (MVM), a common parvovirus used in studying viral clearance in downstream processing in industry [3,10]. To reduce particle-particle interactions, SPT experiments were conducted in the dilute limit, roughly 10^5 pfu/mL. The flow cell system was operated in dead-end mode with a flow rate of 0.001 mL/min, controlled by a syringe pump (Fusion 200, Chemyx Inc.) providing a flow rate of 4.26 $\frac{L}{m^2 h}$ and a Péclet number of 0.27 based on the calculated in-membrane diffusivity. To observe bulk diffusion, the flow cell was simply filled with the solution without using the syringe pump.

The experimental conditions for single particle tracking were based

on those described by Wu et al. [19], with specific enhancements to optimize super-resolution imaging of ΦX174 in the Pegasus SV4 membranes. HILO illumination was used to reduce background fluorescence, and a 2 × zoom was employed to focus the illumination on the membrane area. Non-continuous illumination—activating the light source only 5 s before and after flow interruption— was used to reduce photo-bleaching and improve particle localization during the imaging stages of particular interest.

2.2. Simulation of virus breakthrough during flow interruptions

To simulate the virus breakthrough during periods of flow interruption, we implemented a one-dimensional Monte Carlo simulation. The simulation did not account for interactions among particles, focusing solely on their independent diffusive transport. The simulation was initialized with a membrane spanning 0–30 μm. To mimic the experimental conditions from Afzal and Zydney [3], the feed concentration was set at 3×10^6 pfu/mL, and the in-membrane concentration was adjusted to 10^8 pfu/mL based on the accumulation of retained ΦX174 prior to the process disruption. We initialized 10,000 particles with starting positions at the inlet and within the membrane. The inlet featured a uniform concentration that extended a distance farther than particles could travel during the course of the simulation. The membrane concentration was distributed along the filter depth based on the observed capture profile from Leisi et al. for the retention of MVM inside the Pegasus SV4 membrane evaluated using confocal imaging [11,16].

3. Results

3.1. Characterization of retained bacteriophage populations within pegasus SV4

Single particle tracking was used to analyze the transport of ΦX174 within a single layer of the Pegasus SV4 membrane, enabling successful real-time imaging of virus motion within a viral filtration membrane, as depicted in Fig. 1A. Interestingly, the retention profiles were apparently more consistently dispersed along the filter depth compared to the distinctive reservoir zone seen using confocal imaging. A possible explanation for this could be due to the lower phage loading required for single particle tracking studies in conjunction with the lower volumetric throughput the membrane was challenged with.

During the filtration studies, two distinct populations of apparently retained objects (dubbed immobile and trapped, as described below) were robustly and reproducibly identified using a convex hull algorithm, as shown in Fig. 1B. A small fraction of mobile trajectories was also identified during imaging and are depicted alongside immobile and trapped phage particles in Fig. S3. The convex hull, defined as a polygon of minimum area enclosing a set of points, differentiated mobile particles based on their motion and large spatial trajectories. As the focus of this manuscript involved retention loss during flow interruption, mobile trajectories were not analyzed in detail. Another small fraction of objects observed were totally immobile, likely representing a combination of auto-fluorescent membrane defects or particles that were irreversibly adsorbed/stuck in the membrane. Such objects were seen even in experiments without phage particles, consistent with the presence of ubiquitous fluorescent defects generally observed in single-particle imaging. These objects exhibited very small hull areas representative of the localization error of the imaging system. The threshold for the maximum immobile hull area was set on average at 0.026 ± 0.013 μm^2 based on the upper limit for position uncertainty for each movie. Because differentiation between membrane artifacts and immobilized particles was not feasible, no further analysis was performed on this small subpopulation.

The majority of objects (typically 80–90 %) observed in the experiments with labeled bacteriophage were categorized as trapped particles, which were apparently hydrodynamically constrained within larger

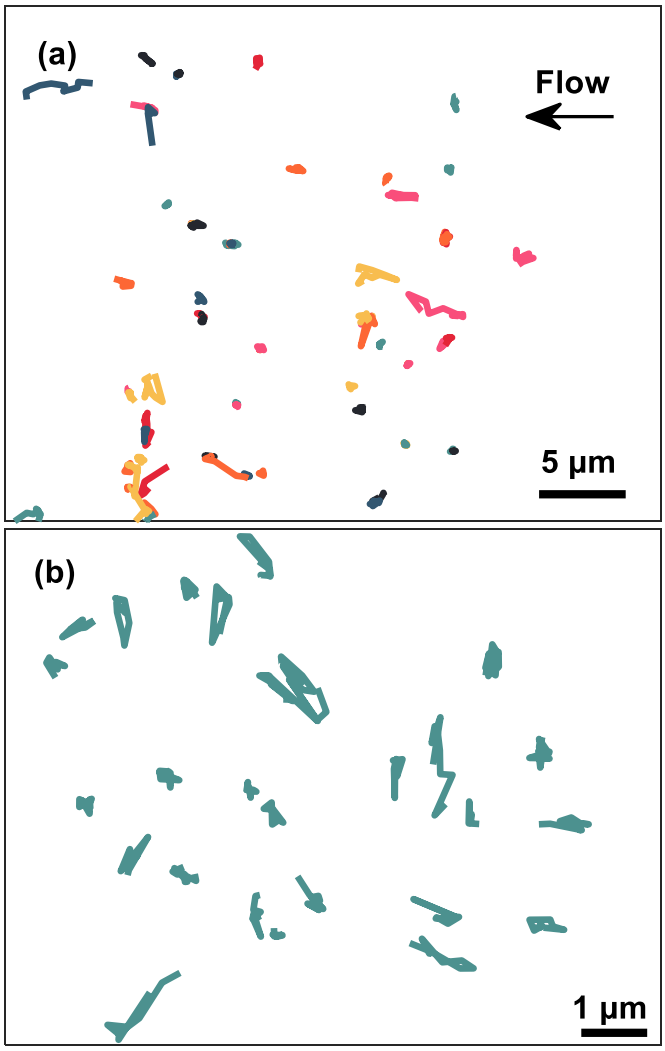

Fig. 1. Two-dimensional trajectories of fluorescently labeled ΦX174 within a single layer of Pegasus SV4 during flow and resumption stages. (a) A region of interest showing all trajectories observed during an experiment with a 2-min disruption interval. Colors are arbitrary and used only to distinguish trajectories. (b) Representative trajectories for the distinct trapped sub-population identified using a convex hull algorithm. Trajectories are randomly distributed and plotted over 0.50 s.

cavities, as described by Yamamoto et al. [7]. These cavities feature exit holes aligned with the flow direction that allow fluid to pass through while preventing translocation of retained particles. These trapped particles were the main focus of subsequent analysis performed. Based on the ratio of advective to diffusive forces, as described by the Péclet number, these particles had some freedom within the membrane cavity space. SPT experiments showed that the average hull area of these trajectories was 0.29 ± 1.1 μm^2, with a heavy-tailed distribution indicating entrapment within an individual cavity, or a collection of neighboring cavities, of varying sizes (Fig. S4). Based on the shapes of these trapped trajectories, and previous measurements of characteristic void dimensions within the SV4 membrane, many of these particles are apparently trapped within contiguous sets of cavities. Characterization of the pore network across different homogenous VF devices reveals a distribution of cavity and hole sizes [6,8]; their specific variances within the Pegasus SV4 membrane is detailed below. On average the trapped fraction was 0.84 ± 0.14; no significant change in retention fractions was observed between flow and resumption stages (Table S1).

We hypothesized that this large trapped-but-dynamic population corresponds to the virus particles that may escape the membrane during

process disruptions, as described by the modified internal polarization model [3,12]. This model suggests that increased volumetric throughput to the membrane leads to the accumulation of particles within the reservoir zone that are, specifically, not irreversibly stuck. When pressure is released, this subpopulation can diffusively explore their environment through non-retentive pathways.

3.2. Bacteriophage remobilization from a cavity is rapid during flow disruption

Flow cell experiments featuring process disruptions were performed to understand the observed macroscopic losses in retention. Process disruptions were conducted in triplicate, with durations ranging from 2 to 10 min. Based on breakthrough measurements [3], the release fraction increased from 3 % to 41 % over this range of flow stoppage times, following process resumption. Thus, this range of stoppage times was expected to be highly relevant to the processes causing the macroscopic retention loss.

In SPT experiments, the fraction of particles retained after a flow stoppage event was determined by comparing the localization coordinates of trajectories during the initial flow and resumption stages.

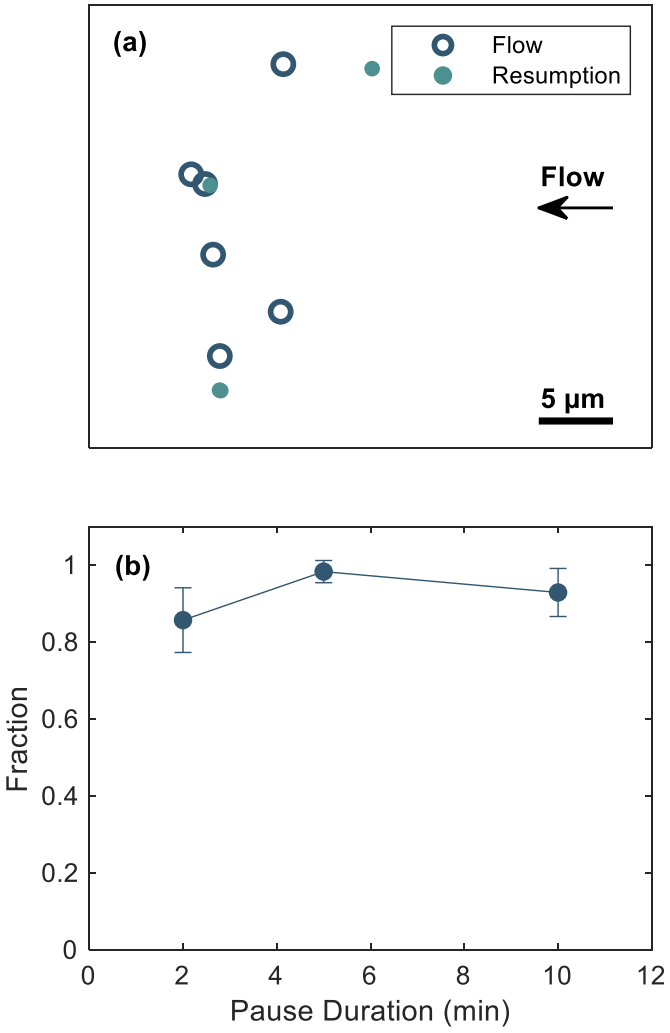

Fig. 2. Remobilization from a single pore space. (a) A representative region of a remobilization map from a single movie featuring a 2-min pause duration. The average position of trapped particles from flow and resumption stages are plotted. Strong overlap implies retention of the same particle. (b) The remobilization fraction determined using a nearest neighbor search algorithm as a function of disruption duration.

This comparison, depicted in Fig. 2A, involved using a nearest neighbor search algorithm to verify whether a trapped particle during the initial stage had a corresponding trajectory following process disruption within a Euclidean distance threshold. These data allowed us to identify remobilized particles and to calculate the apparent remobilization fraction.

Interestingly, unlike the substantial monotonic increase of the macroscopic release fraction with process disruption duration (from 2 to 10 min) seen in virus breakthrough curve experiments [3], the microscopic remobilization fraction was large over the entire range of time intervals and displayed no significant trend (Fig. 2B), ranging from 0.86 $\pm$ 0.08 to 0.98 $\pm$ 0.03, suggesting possible saturation of remobilization events. A one-way analysis of variance (ANOVA) for the remobilization fraction across each disruption interval returned a p-value of 0.122, suggesting that the remobilization was either complete or nearly complete after only 2 min. Importantly, this result suggests that the escape of phage particles from their original retention location was not the rate-limiting process associated with subsequent release after flow resumption. This is in stark contrast to the remobilization of polystyrene nanoparticles in filtration membranes with larger sub-μm pores observed by Wu et al. [19]. In their study, the remobilization fraction increased monotonically with pause time, and a clear initial movement of remobilized particles against the flow direction was observed, suggesting the diffusive escape of particles retained in constricting elements of the pore network. We speculate that the qualitative difference in these findings between the two systems is due to the much smaller characteristic size of structures within virus filtration membranes. In a membrane with larger structures, diffusive escape from the location/cavity of retention is slow and determines the characteristic stoppage time required for release after flow resumption. In contrast, in a virus filtration membrane with extremely small cavities, diffusive escape from a local cavity occurs extremely rapidly, and apparently does not represent a key limiting process leading to loss of retention. These observations imply that while apparent remobilization is a necessary precondition for viral breakthrough, it is not the rate-limiting step. In particular, the apparent remobilization from a retaining void space saturates at times earlier than 2 min, which is much faster than the stoppage times required for significant loss of retention. Additionally, when flow resumes, the retentive properties of the system are immediately restored [3,9]. Given the complex, interconnected, and tortuous nature of VF devices, we hypothesize that particles must diffuse characteristic length scales equal to or greater than the membrane thickness before flow resumes to achieve breakthrough.

3.3. Diffusion of bacteriophage is hindered yet substantial within the membrane during flow disruption

To investigate the transport properties of viruses within the Pegasus SV4 membrane during flow interruption, diffusion studies were conducted in RI matching media under stagnant conditions. The mean square displacements (MSD) of particle trajectories were analyzed using a combination of in-house tracking software and open-source analysis tools [23]. Fig. 3A displays representative phage trajectories within the Pegasus SV4, where transport was significantly hindered. The motion of phage particles within the membrane was apparently Brownian, with a diffusion coefficient approximately thirty times smaller than in bulk (unconfined) liquid. The static tortuosity of the membranes under these conditions was ~5.5, but due to the process dependent nature of tortuosity, apparently varies under differing flow and solution conditions [21]. The measured bulk diffusion coefficient, 4.19 $\pm$ 0.06 $\mu m^2/s$, was faster than expected based on the nominal solution viscosity and particle size, suggesting a deviation from the Stokes-Einstein relation due to possible surface slip in the RI matching fluid. This phenomenon was further characterized by diffusion experiments on nominally 20 nm fluorescent tracers in both RI matching and aqueous solutions, as detailed in Fig. S5.

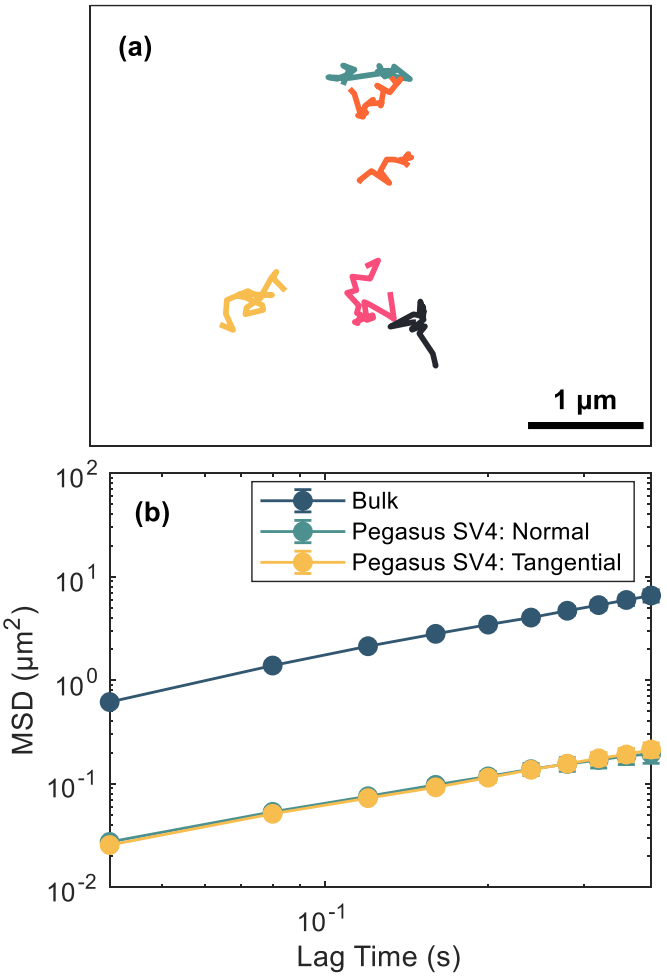

Fig. 3. Diffusion of ΦX174 within the RI matching solution under stagnant conditions. (a) Representative trajectories of phage within a Pegasus SV4 membrane plotted over 0.80 s. (b) MSD plots of particles within membranes show significant hindrance from bulk diffusion. No difference was observed between diffusion normal or tangential to the nominal flow direction within the membrane.

Importantly, within the confining environment, diffusion was quasi-Fickian and isotropic as indicated in Fig. 3B. A power law analysis of the MSD with respect to lag time exhibited only slightly sub-diffusive behavior over long timescales. The anomalous exponent was 0.91 ± 0.02 for intra-membrane diffusion allowing us to extract an effective Fickian diffusion coefficient of 0.139 ± 0.004 $\mu m^2/s$ via linear regression. Additionally, changing the orientation of the membrane sample to study diffusion tangential and normal to the nominal flow direction showed no difference in transport behavior. Fig. 3B depicts the MSD data for representative trajectories inside and outside of the Pegasus SV4 membrane. This Fickian and isotropic behavior over long timescales suggests a macroscopic random walk from neighboring cavities through the membrane's pore network [24]. This behavior indicates that many constrictions within the porous network are larger than the phage particle, allowing diffusive exploration. Indeed, Russell et al. used FIB-SEM to characterize the pore network and found that only 15 % of holes within the pore network were smaller than 20 nm [8], the reported pore size of the membrane, consistent with easy access of virus to the porous environment in the absence of advection. Moreover, the cavity size was shown to vary from 70 nm to 120 nm [8]. For clarity, SEM images of the membrane structure can be found in Fig. S2. Based on the measured diffusivity within the membrane, a phage particle would require only 26 ms to travel a distance equivalent to the upper limit of the physical cavity size, consistent with the saturation of the remobilization phenomena observed in other porous media systems [18]. This short pore-escape time thus explains the rapid saturation of remobilized trapped particles at the studied timescales as described above. Importantly, during a process disruption of 30 min, a virus can traverse characteristic distances of approximately 31 μm within the porous medium (in the RI-matching liquid), which is slightly longer than the thickness of the entire membrane [8]. Under normal operating conditions with reduced viscosity, the particles can diffuse even farther.

3.4. Connecting macroscopic retention losses with transmembrane diffusion during process disruptions

Various mechanisms have been ascribed for the retention loss due to flow stoppage. Initial observations suggested that flow stoppage might induce structural changes or damage within filtration devices, potentially leading to particle release [12]. However, the first quantitative study by Woods and Zydney [12] challenged these assumptions, demonstrating that resumption of flow restored normal operating conditions. A current working hypothesis within the field is based on virus diffusion; during periods of flow stoppage, virus particles can diffuse laterally away from where they are retained, allowing deeper migration into the membrane [3,4,7,10,12,16]. Within this framework, it has generally been assumed that the resumption of flow is required for particle breakthrough to occur. Lacasse et al. [10] specifically hypothesized that this diffusive mechanism operates on length scales of 1–15 μm but does not exceed the membrane thickness. These ideas are based on ensemble level data, where increased phage concentrations in the collected permeate and deeper penetration of the retentive band have been observed in homogenous filters following flow resumption.

Contrary to these observations, our single particle tracking data suggest that phage diffusion within the Pegasus SV4 membrane can significantly exceed these limits during typical process disruption intervals, allowing particles to traverse distances equal to or greater than the entire filter thickness. Therefore, we speculate that while the resumption of flow might aid virus breakthrough for retained particles near the filter exit, it is not an essential part of the underlying mechanism. Instead, long-term diffusion alone is sufficient for membrane escape to occur. Additionally, the extensive distances traveled by phage particles during disruptions imply that not only retained virus particles, but also those within the feed solution immediately adjacent to the virus filter, can be released into the filtrate through diffusion. This observation implies that a 100 % release fraction does not represent a definitive upper limit.

To connect the macroscopically observed losses in viral retention, as noted by Afzal and Zydney [3], we performed one-dimensional Monte Carlo simulations based on the experimental in-membrane diffusivity. To accurately represent the observed losses in virus retention in the system featuring a PBS solution, the bulk diffusion coefficient was adjusted based on the ratio of diffusivities of tracer particles in the RI and aqueous solutions, as shown in Fig. S5. As such, the diffusion coefficient was set to 30.4 $\mu m^2/s$ for areas outside of the membrane. Due to the inherent complexity of the membrane pore-space, the in-membrane diffusivity may not necessarily scale by the same factor. The diffusion of phage within the PBS-Pegasus SV4 system was therefore estimated by minimizing the sum of squared errors between simulation data and experimental findings (Fig. S6). A more detailed description of the simulation can be found within the Supporting Information. The resultant diffusivity is 0.417 $\mu m^2/s$, hindered by a factor of 73 from the bulk. Consequently, we estimated that particles can diffusive a characteristic distance of 55 μm in PBS during a 30-min disruption interval within the pore network, 1.83 times the single layer membrane thickness.

Throughout the simulation, notable changes in the retention profile of particles were observed within the membrane, extending 0–30 μm in filter depth (Fig. 4A). Initially, particles were trapped primarily near the inlet with a characteristic profile indicative of the reservoir zone. At

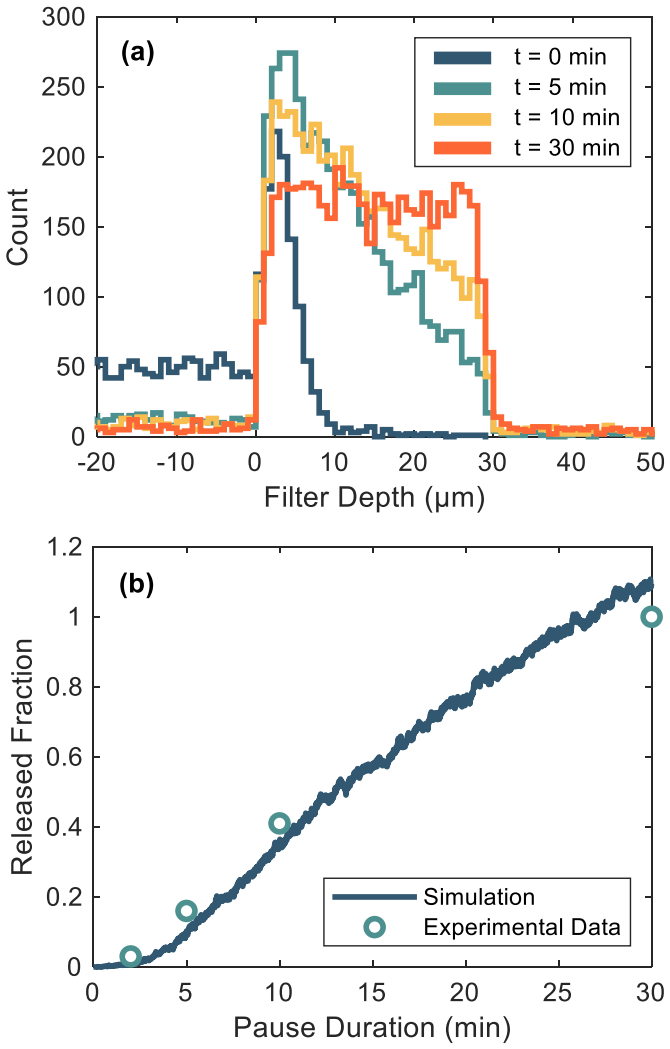

Fig. 4. Monte-Carlo Simulation for virus release during a process disruption. (a) Particle positions near the membrane region over the course of the simulation. (b) Optimized simulation parameters that are in good agreement with the experimental work by Afzal and Zydney [3]. The optimized parameter value for the in-membrane phage diffusivity is $\boldsymbol{D_{mem}} = \mathbf{0.417}\frac{\mu m^2}{s}$; a more detailed description of how this value was chosen can be found in the SI.

short times (5 min), little remobilization was observed yet strong polarization of the reservoir layer was present, as evidenced by increased particle counts within the membrane and a similar retention profile to that at the simulation start. At longer times, the retention profile approached a steady-state, and a broadening of the characteristic retention band was observed. At the final simulation timepoint, the capture profile was approximately uniform, in part due to substantial differences between bulk and membrane diffusivities.

Based on these profiles, rapid mitigation of flow stoppage is crucial to limit downstream viral contamination. Manufacturers may employ a combination of process control and membrane design strategies, such as specialty valves for seamless process transitions and membranes with more uniform pore sizes, to enhance robustness [7,10]. Careful design and characterization of the membrane pore network, with specific emphasis on the interconnectivity of cavities, the orientation of constrictive elements, and tortuosity of non-retentive pathways through FIB-SEM and data-science-based reconstructions can facilitate more effective filtration strategies [6,8].

Fig. 4B illustrates the release fraction as a function of process disruption interval, with stoppage times ranging from 0 to 30 min. The simulation data closely align with macroscopic experimental observations. Interestingly, only 17 % of particles released to the filtrate originated from the membrane; the simulation started with 11 % of the total particles therein. Additionally, 82 % of particles initially within the membrane remained there after a 30-min disruption. This study confirms our hypothesis that the resumption of flow is not necessary for virus release, underscoring a diffusive mechanism driven by long-time macroscopic diffusion through the porous membrane structure.

4. Conclusions

In the biopharmaceutical industry, the removal of viral contaminants is crucial for ensuring product safety and process integrity. Virus filters play a critical role in the virus clearance strategy by offering a size-based exclusion route of removal. The efficacy of these highly engineered VF devices is notably process-dependent, with deviations from standard operating procedures significantly reducing virus retention within the porous structure under some conditions. Given that process disruptions are practically unavoidable in industry, understanding the mechanisms of virus release during these disruptions is essential.

In this study, we utilized single particle tracking and simulation to link macroscopic retention losses observed at the ensemble level with individual particle behavior during flow interruption. The methods employed resulted in the first observations of individual phage transport and retention within the membrane. We observed that during filtration, most retained particles were trapped, but fluctuated dynamically within cavities or groups of contiguous cavities. Upon flow disruption, immediate remobilization of trapped particles occurred before any significant viral fraction could be released. Diffusion experiments under stagnant conditions indicated significant hindrance within the membrane; however, particles were still able to traverse considerable distances on timescales where retention losses were observed. This is a direct result of the distribution of cavity and hole sizes in polymeric membrane materials, which create tortuously connected, non-retentive pathways that are otherwise inaccessible during periods of flow. Even in the more viscous (refractive index matching) solution, the characteristic distance traveled was on the same order of magnitude as the single-layer thickness of the Pegasus SV4 membrane.

By employing a simple 1D Monte Carlo simulation, we connected single particle dynamics to ensemble-level motion. It has long been suggested that the mechanism for this process involved diffusive exploration of the membrane's pore space. However, our work suggests a new mechanism that distinctly omits the resumption of flow for breakthrough. Instead, our findings indicate that phages can diffuse sufficient lengths to enable transport into the filtrate in the total absence of convective forces (although the virus may not be carried far enough to be observed in the collected permeate until the filtration flow is resumed). These insights, elucidated by single particle tracking, offer a framework for the mitigation and rational design of future process conditions and membrane structures to enhance the performance of virus removal filtration processes.

Funding sources

Support for this work was provided through the Membrane Applications Science and Technology (MAST) Center, which is funded by grant numbers 1624602, 1841474, and 2310832 from the NSF IUCRC program.

CRediT authorship contribution statement

Ian Wyllie: Writing – original draft, Software, Investigation, Formal analysis, Data curation, Conceptualization. **Mohammad A. Afzal:** Writing – review & editing, Resources, Conceptualization. **Anni Shi:** Writing – review & editing, Software, Methodology, Conceptualization. **Andrew L. Zydney:** Writing – review & editing, Supervision, Project

administration, Methodology, Funding acquisition, Conceptualization. **Daniel K. Schwartz:** Writing – review & editing, Supervision, Project administration, Methodology, Funding acquisition, Conceptualization.

Declaration of competing interest

The authors declare the following financial interests/personal relationships which may be considered as potential competing interests.

Daniel K. Schwartz & Andrew L. Zydney report financial support was provided by National Science Foundation Industry-University Cooperative Research Centers Program. If there are other authors, they declare that they have no known competing financial interests or personal relationships that could have appeared to influence the work reported in this paper.

Data availability

Data will be made available on request.

Acknowledgment

Support was proviced through the Membrane Applications Science and Technology (MAST) Center, which is funded by grant numbers 1624602, 1841474, and 2310832 from the NSF IUCRC program. The imaging work was performed at the BioFrontiers Institute Advanced Light Microscopy Core (RRID: SCR_018302). HILO microscopy was performed on a Nikon Ti-E microscope supported by the Howard Hughes Medical Institute.

During the preparation of this work the authors used ChatGPT in order to improve language and readability of an initial draft. After using this tool, the authors reviewed and edited the content extensively and take full responsibility for the content of the publication.

Appendix A. Supplementary data

Supplementary data to this article can be found online at https://doi.org/10.1016/j.memsci.2024.123380.

References

[1] S. Isu, X. Qian, A.L. Zydney, S.R. Wickramasinghe, Process- and product-related foulants in virus filtration, Bioengineering 9 (2022) 155, https://doi.org/10.3390/bioengineering9040155.

[2] Y. El Abd, A. Tabll, R. Smolic, M. Smolic, Mini-review: the market growth of diagnostic and therapeutic monoclonal antibodies – SARS CoV-2 as an example, Hum. Antibodies 30 (2022) 15–24, https://doi.org/10.3233/HAB-211513.

[3] M.A. Afzal, A.L. Zydney, Effect of filtrate flux and process disruptions on virus retention by a relatively homogeneous virus removal membrane, Biotechnol. Prog. 38 (2022) e3255, https://doi.org/10.1002/btpr.3255.

[4] S.K. Dishari, A. Venkiteshwaran, A.L. Zydney, Probing effects of pressure release on virus capture during virus filtration using confocal microscopy, Biotechnol. Bioeng. 112 (2015) 8.

[5] N.B. Jackson, M. Bakhshayeshi, A.L. Zydney, A. Mehta, R. Van Reis, R. Kuriyel, Internal virus polarization model for virus retention by the Ultipor ® VF Grade DV20 membrane, Biotechnol. Prog. 30 (2014) 856–863, https://doi.org/10.1002/btpr.1897.

[6] H. Chamani, A. Rabbani, K.P. Russell, A.L. Zydney, E.D. Gomez, J. Hattrick-Simpers, J.R. Werber, Data-science-based reconstruction of 3-D membrane pore structure using a single 2-D micrograph, J. Membr. Sci. 678 (2023) 121673, https://doi.org/10.1016/j.memsci.2023.121673.

[7] A. Yamamoto, T. Hongo-Hirasaki, Y. Uchi, H. Hayashida, F. Nagoya, Effect of hydrodynamic forces on virus removal capability of Planova^{TM} filters, AIChE J. 60 (2014) 2286–2297, https://doi.org/10.1002/aic.14392.

[8] K.P. Russell, A.L. Zydney, E.D. Gomez, Impact of virus filter pore size/morphology on virus retention behavior, J. Membr. Sci. 670 (2023) 121335, https://doi.org/10.1016/j.memsci.2022.121335.

[9] M.A. Afzal, A.L. Zydney, Impact of proteins and protein fouling on virus retention during virus removal filtration, Biotechnol. Bioeng. 121 (2024) 710–718, https://doi.org/10.1002/bit.28607.

[10] D. LaCasse, S. Lute, M. Fiadeiro, J. Basha, M. Stork, K. Brorson, R. Godavarti, C. Gallo, Mechanistic failure mode investigation and resolution of parvovirus retentive filters, Biotechnol. Prog. 32 (2016) 959–970, https://doi.org/10.1002/btpr.2298.

[11] R. Leisi, E. Widmer, B. Gooch, N.J. Roth, C. Ros, Mechanistic insights into flow-dependent virus retention in different nanofilter membranes, J. Membr. Sci. 636 (2021) 119548, https://doi.org/10.1016/j.memsci.2021.119548.

[12] M.A. Woods, A.L. Zydney, Effects of a pressure release on virus retention with the Ultipor DV20 membrane, Biotechnol. Bioeng. 111 (2014) 545–551, https://doi.org/10.1002/bit.25112.

[13] S. Lute, M. Bailey, J. Combs, M. Sukumar, K. Brorson, Phage passage after extended processing in small-virus-retentive filters, Biotechnol. Appl. Biochem. 47 (2007) 141–151, https://doi.org/10.1042/BA20060254.

[14] G. Bolton, M. Cabatingan, M. Rubino, S. Lute, K. Brorson, M. Bailey, Normal-flow virus filtration: detection and assessment of the endpoint in bioprocessing, Biotechnol. Appl. Biochem. 42 (2005) 133, https://doi.org/10.1042/BA20050056.

[15] M. Bieberbach, P. Kosiol, A. Seay, M. Bennecke, B. Hansmann, S. Hepbildikler, V. Thom, Investigation of fouling mechanisms of virus filters during the filtration of protein solutions using a high throughput filtration screening device, Biotechnol. Prog. 35 (2019) e2776, https://doi.org/10.1002/btpr.2776.

[16] R. Leisi, I. Rostami, A. Laughhunn, J. Bieri, N.J. Roth, E. Widmer, C. Ros, Visualizing protein fouling and its impact on parvovirus retention within distinct filter membrane morphologies, J. Membr. Sci. 659 (2022) 120791, https://doi.org/10.1016/j.memsci.2022.120791.

[17] F. Namila, D. Zhang, S. Traylor, T. Nguyen, N. Singh, S.R. Wickramasinghe, X. Qian, The effects of buffer condition on the fouling behavior of MVM virus filtration of an Fc-fusion protein, Biotechnol. Bioeng. 116 (2019) 2621–2631, https://doi.org/10.1002/bit.27085.

[18] Y. Cai, D.K. Schwartz, Single-nanoparticle tracking reveals mechanisms of membrane fouling, J. Membr. Sci. 563 (2018) 888–895, https://doi.org/10.1016/j.memsci.2018.06.044.

[19] H. Wu, Y. Cai, D.K. Schwartz, Particle remobilization in filtration membranes during flow interruption, J. Membr. Sci. 610 (2020) 118405, https://doi.org/10.1016/j.memsci.2020.118405.

[20] H. Wu, D.K. Schwartz, Nanoparticle tracking to probe transport in porous media, Acc. Chem. Res. 53 (2020) 2130–2139, https://doi.org/10.1021/acs.accounts.0c00408.

[21] Y. Cai, D.K. Schwartz, Mapping the functional tortuosity and spatiotemporal heterogeneity of porous polymer membranes with super-resolution nanoparticle tracking, ACS Appl. Mater. Interfaces 9 (2017) 43258–43266, https://doi.org/10.1021/acsami.7b15335.

[22] H. Wu, A. Kanora, D.K. Schwartz, Fouling of microfiltration membranes by bidisperse particle solutions, J. Membr. Sci. 641 (2022) 119878, https://doi.org/10.1016/j.memsci.2021.119878.

[23] N. Tarantino, J.-Y. Tinevez, E.F. Crowell, B. Boisson, R. Henriques, M. Mhlanga, F. Agou, A. Israël, E. Laplantine, TNF and IL-1 exhibit distinct ubiquitin requirements for inducing NEMO–IKK supramolecular structures, J. Cell Biol. 204 (2014) 231–245, https://doi.org/10.1083/jcb.201307172.

[24] H. Wu, D. Wang, D.K. Schwartz, Connecting hindered transport in porous media across length scales: from single-pore to macroscopic, J. Phys. Chem. Lett. 11 (2020) 8825–8831, https://doi.org/10.1021/acs.jpclett.0c02738.